Yang and Lee *Nanoscale Research Letters* (2017) 12:582
DOI 10.1186/s11671-017-2355-7

Nanoscale Research Letters

NANO EXPRESS Open Access

Determining the Catalytic Activity of Transition Metal-Doped TiO_2 Nanoparticles Using Surface Spectroscopic Analysis

Sena Yang[1] and Hangil Lee[2*]

Abstract

The modified TiO_2 nanoparticles (NPs) to enhance their catalytic activities by doping them with the five transition metals (Cr, Mn, Fe, Co, and Ni) have been investigated using various surface analysis techniques such as scanning electron microscopy (SEM), Raman spectroscopy, scanning transmission X-ray microscopy (STXM), and high-resolution photoemission spectroscopy (HRPES). To compare catalytic activities of these transition metal-doped TiO_2 nanoparticles (TM-TiO_2) with those of TiO_2 NPs, we monitored their performances in the catalytic oxidation of 2-aminothiophenol (2-ATP) by using HRPES and on the oxidation of 2-ATP in aqueous solution by taking electrochemistry (EC) measurements. As a result, we clearly investigate that the increased defect structures induced by the doped transition metal are closely correlated with the enhancement of catalytic activities of TiO_2 NPs and confirm that Fe- and Co-doped TiO_2 NPs can act as efficient catalysts.

Keywords: Transition metal-doped TiO_2, Catalytic activity, HRPES, STXM, EC measurements

Background

For several decades, it has been well known that titanium oxide (TiO_2) has an effective catalytic activity as well as low cost, so TiO_2 has received significant attention because of its various applications in solar cells, photocatalysis, and electrochemical catalysis [1–7]. Although TiO_2 is a promising material, the TiO_2 (rutile or anatase structures) has relatively wide band gap (E_g = 3.0~3.2 eV), and this width allows it to absorb only UV light. Therefore, significant efforts have been applied toward narrowing its band gap and enhancing catalytic activity. For this reason, an insertion of foreign elements as dopants has been widely performed to narrow the bandgap since the impurity element in TiO_2 can modify band edge states.

Hence, our strategy is to insert transition metals as dopants into TiO_2 NPs to enhance the catalytic performance of TiO_2 NPs significantly, because they can increase the defect structures of TiO_2 NPs, which is closely related to the enhancement of catalytic activity [8–18]. To further study from previous researches [19, 20], we performed the insertion of various transition metal ions (TM^+) into TiO_2 and then compared catalytic activities of the TiO_2 NPs containing the various transition metal dopants with those TiO_2 NPs. From this, we can assess the effectiveness of transition metal dopants for TiO_2 NPs and compare photocatalytic activities between various transition metals together.

In our study, we successfully fabricated the five transition metal-doped TiO_2 NPs (TM-TiO_2; TM=Cr, Mn, Fe, Co, and Ni) with a thermo-synthesis process (see the "Methods" section). We first compared the morphologies and electronic properties of the five TM-TiO_2 with TiO_2 NPs by using scanning electron microscopy (SEM), Raman spectroscopy, and scanning transmission X-ray microscopy (STXM). And then, we assessed their catalytic capacities by oxidizing 2-aminothiophenol (2-ATP) under ultra-high vacuum (UHV) conditions (a base pressure below 9.5×10^{-11} Torr) with 365 nm UV light illumination using high-resolution photoemission spectroscopy (HRPES), and cyclic voltammogram (CV) changes in the solution phase by using electrochemistry. These reactions and analyses were also

* Correspondence: easyscan@sookmyung.ac.kr
[2]Department of Chemistry, Sookmyung Women's University, Seoul 140-742, Republic of Korea
Full list of author information is available at the end of the article

performed to determine the mechanism of the catalytic oxidation reaction.

Methods

Preparation of the Precursor Solutions

We prepared each precursor solution with a one pot synthesis. The desired amounts of the transition metal dopants (TM) were added in the form $TM(NO_3)_x{\cdot}nH_2O$ (metal nitrate *n*-hydrate; TM=Cr, Mn, Fe, Co, or Ni) as mole fractions with respect to TiO_2 ($TM/(TM+TiO_2)$), which were used as the dopants. All substances were purchased from Sigma-Aldrich. The precursor solutions are stirred for 10 min. 2-Aminothiophenol (2-ATP, Sigma Aldrich, 97% purity) and Nafion (Sigma Aldrich, 5 wt% in a low-molecular-weight aliphatic alcohol and water) were purchased from Sigma-Aldrich. Phosphate-buffered saline (PBS) tablets are purchased from Gibco.

Preparation of the Dispersed TM-TiO_2 Solutions

Tetramethylammonium hydroxide (TMAOH) (1.2 g) was diluted with double-distilled water (DDW, 22.25 g). Titanium isopropoxide (TTIP, 3.52 g) was diluted with isopropanol (3.5 g). Both of these solutions were stirred separately for 10 min. White TiO_2 appeared by adding the TTIP solution dropwise to the TMAOH solution at room temperature. And then, the desired amounts (5 mol%) of the transition metal dopants were added to each synthetic gel solution in an oil bath at 80 °C with stirring. After approximately 10 min, the synthetic gel solution became a transparent solution. The solutions were transferred to Teflon-lined autoclaves and then heated at 220 °C for 7 h in a convection oven. The resulting TM-TiO_2 (Cr-TiO_2, Mn-TiO_2, Fe-TiO_2, Co-TiO_2, and Ni-TiO_2) were filtered and washed with DDW to remove any residue.

Fabrication of TM-TiO_2-Nafion-Modified GCE and Electrochemical Measurements of 2-ATP Oxidation

The electrochemical oxidation of 2-ATP was investigated using glassy carbon electrodes (GCEs) modified with TM-TiO_2. For each TM, a mass of 4.0 mg of TM-TiO_2 was dispersed into 2.0 ml of distilled water containing 50 μl Nafion, and then mixed by using an ultrasonic processor for 5 min to obtain the homogeneous TM-TiO_2-Nafion mixture. After that, a volume of 20 μl of the mixture was placed on a GCE and was dried at 80 °C in a pre-heated oven for 30 min. A cyclic voltammogram (CV) of 0.01 M 2-ATP in PBS was obtained for each TM-TiO_2-Nafion modified GCE.

Characterizations

The morphology and size distribution of the fabricated nanoparticles was analyzed by using field-emission scanning electron microscopy (FE-SEM, FEI Inspect F50, operating at 10 kV). Raman spectra were obtained by using a spectrometer (Horiba, ARAMIS) with an Ar^+

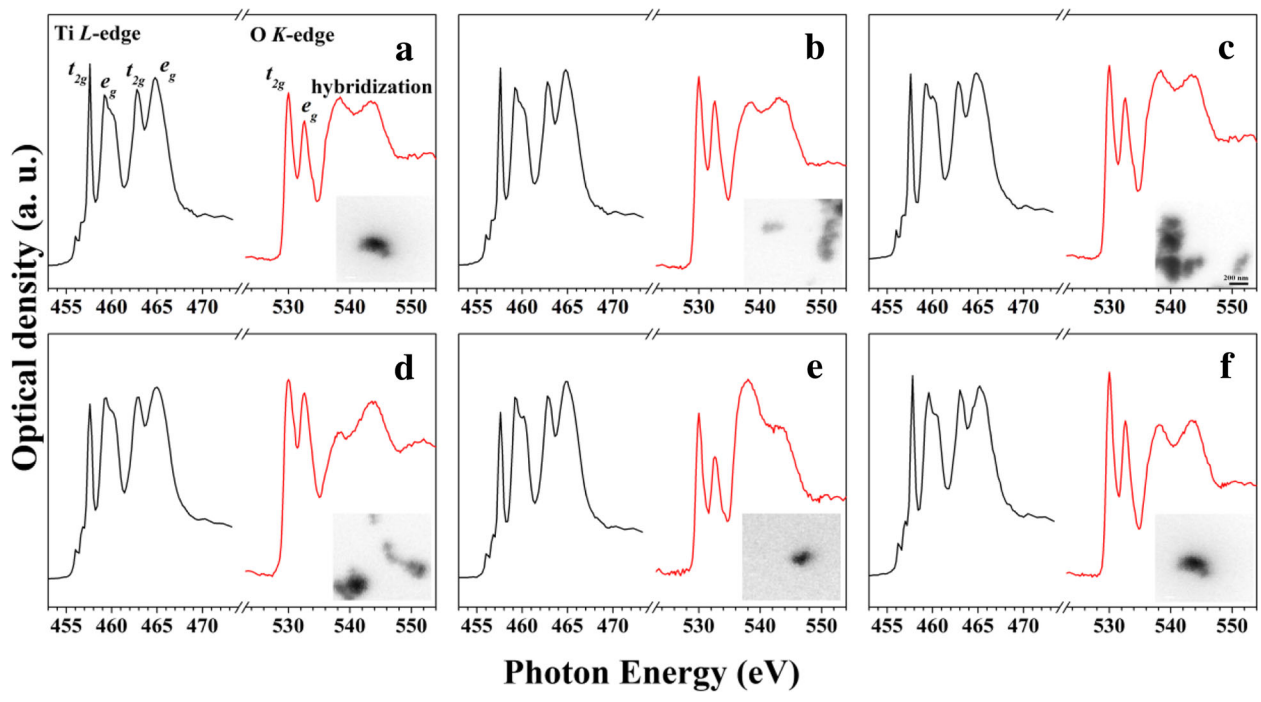

Fig. 1 XAS spectra (Ti $L_{2,3}$-edge and O *K*-edge) and the corresponding stacked images for **a** anatase TiO_2, **b** Cr-TiO_2, **c** Mn-TiO_2, **d** Fe-TiO_2, **e** Co-TiO_2, and **f** Ni-TiO_2 (5 mol% TM-TiO_2 NPs). The stacked image size is 1 μm × 1 μm (scale bar is 200 nm)

ion CW (514.5 nm) laser. Scanning transmission X-ray microscopy (STXM) results with a 25-nm resolution were obtained at the 10A beamline of the Pohang Accelerator Laboratory (PAL). STXM was used to obtain image stacks by using X-ray absorption spectroscopy (XAS) to elicit the doped transition metal *L*-edge, Ti *L*-edge, and O *K*-edge spectra. High-resolution photoemission spectroscopy (HRPES) experiments were carried out on an electron analyzer (SES-100, Gamma-Data Scienta) at the 8A2 beamline of PAL to identify the electronic structure. The S 2*p* core level spectra were recorded with an electron energy analyzer. A GCE with a diameter of 2 mm was used as the working electrode and a Pt wire with a diameter of 1 mm was used as the counter electrode, while the reference electrode was Ag/AgCl (3 M KCl).

Results and Discussion

To obtain more detailed characterizations of the electronic structures, we firstly obtained the Ti *L*-edge and O *K*-edge X-ray adsorption spectra (XAS) for TiO_2 NPs and the five TM-TiO_2 (Fig. 1) by using STXM. The black regions of the inset images shown in Fig. 1a–f are originated from TiO_2 NPs and TM-TiO_2. Firstly, the shape of the e_g orbital located at ~ 460 eV for the Ti $L_{2,3}$-edge XAS spectra indicates the presence of typical anatase TiO_2 structure in all TiO_2 NPs and the five TM-TiO_2 [21]. However, when TiO_2 NPs are doped with Fe^{3+} (Fig. 1d) and Co^{3+} ion (Fig. 1e), the ratio of the intensities of the peaks t_{2g} (457.4 eV) and e_g (459~460 eV) decreases below those of the anatase TiO_2 and other TM-TiO_2 (Cr-TiO_2, Mn-TiO_2, and Ni-TiO_2), which indicates the presence of a weak crystal field or an increment in the number of under-coordinated Ti atoms. In other words, these differences are due to the different dopants, which produce different defect structures in the nanoparticles. The small doublets at 456.0 and 456.6 eV in these figures correspond to the Ti^{3+} state; it is well known that metal doping enhances the surface defect structure [22, 23]. The O *K*-edge XAS spectra of the TiO_2 NPs and five TM-TiO_2 contain four peaks at 529.9, 532.3, 537.9, and 543.7 eV [24, 25]. As mentioned in the introduction, the principal purpose of this study is to investigate the electronic states of the TM-TiO_2 and the effects on their catalytic activities. Interestingly, the O *K*-edge spectra show a quite different electronic structure depending on the transition metal dopants. As shown in O *K*-edges, peaks are due to the transition from the O 1*s* state to the unoccupied *p* state,

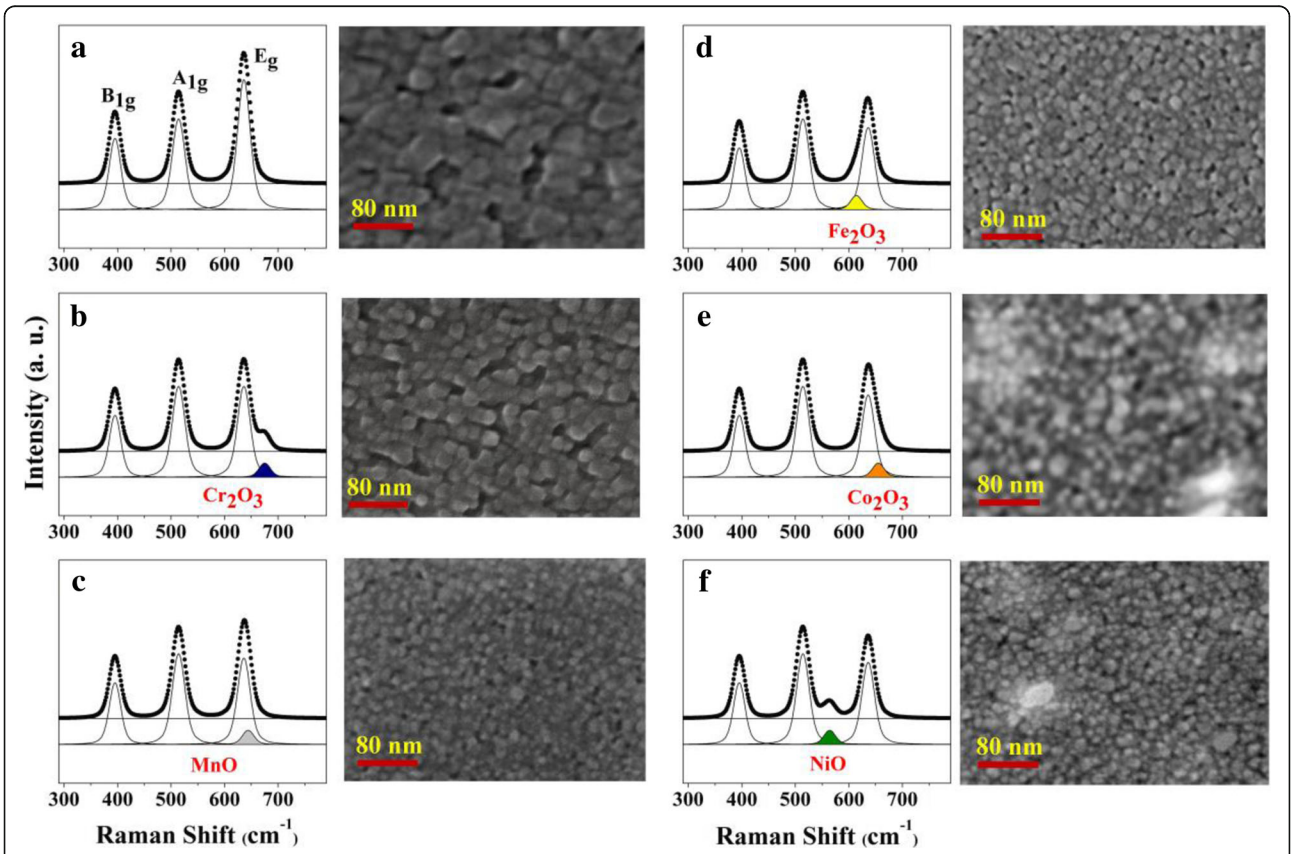

Fig. 2 The Raman spectra of monodisperse 5 mol% TM-TiO_2: **a** anatase TiO_2, **b** Cr-TiO_2, **c** Mn-TiO_2, **d** Fe-TiO_2, **e** Co-TiO_2, and **f** Ni-TiO_2 and the corresponding SEM images, respectively

and from the O 2*p* state to the O 2*p*–Ti 3*d* hybrid orbital state, respectively. The shapes and intensities of the O *K*-edge peaks for Cr-TiO_2, Mn-TiO_2, and Ni-TiO_2 are very similar to those for anatase TiO_2 NPs. However, the O *K*-edges of Fe-TiO_2 and Co-TiO_2 indicate less of the hybrid orbital (538 and 543 eV) than of the bare O 2*p* transition (532.6 eV). In other words, the orbitals of Fe and Co dopants are less hybridized with the O 2*p* orbital including TiO_2 according to the spectra, which is related to catalytic activities and will be discussed again.

We also measured the Raman spectra of TiO_2 NPs and the five TM-TiO_2. As shown in Fig. 2, the electronic structures among TM-TiO_2 are also found to differ, compared with anatase TiO_2 modestly, according to the Raman spectroscopic results. The six samples yield Raman shifts at about 395 (B_{1g}), 514 (A_{1g}), and 636 cm^{-1} (E_g), and they indicate typical anatase TiO_2 peaks [26]. Additionally, we found that each samples show doped transition metal-induced peaks (Cr_2O_3: 675.3 cm^{-1}, MnO: 644.5 cm^{-1}, Fe_2O_3: 614.2 cm^{-1}, Co_2O_3: 657.1 cm^{-1}, and NiO: 564.8 cm^{-1}). Interestingly, we figured out that the doped transition metal ions were changed into the stable metal oxide forms, and the intensity of E_g peak of TiO_2 NPs was a bit lower for TM-TiO_2 than for anatase TiO_2 NPs. We also acquired the SEM (Fig. 2) images of the TiO_2 NPs and the five TM-TiO_2 to determine their surface morphologies. The SEM images show that they have different structural features and sizes. Cr-TiO_2, Mn-TiO_2, Fe-TiO_2, Co-TiO_2, and Ni-TiO_2 have uniform round or rectangular shapes with sizes of ~ 26, ~ 10, ~ 15, ~ 18, and ~ 16 nm, respectively. These five TM-TiO_2 (TM=Cr, Mn, Fe, Co, and Ni) are significantly smaller than the anatase TiO_2 NPs (~ 40 nm: Fig. 2a). Hence, it is possible that the Cr, Mn, Fe, Co, and Ni ions can modify the structure of the TiO_2 NPs and then can act as nucleation sites that assist the formation of fine particles.

In order to examine the modified electronic states induced by the transition metal dopants in more detail, we recorded the transition metal *L*-edge XAS spectra.

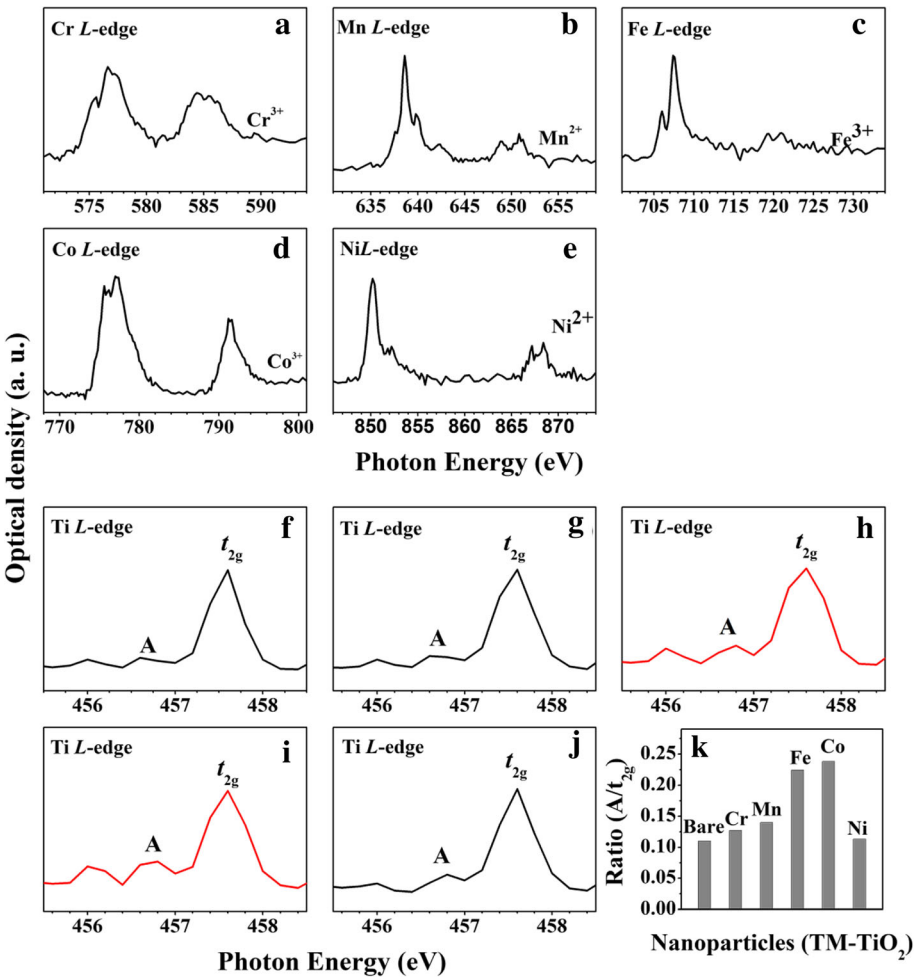

Fig. 3 The doped transition metal *L*-edge and Ti *L*-edge XAS spectra of 5 mol% TM-TiO_2: **a** and **f** Cr-TiO_2, **b** and **g** Mn-TiO_2, **c** and **h** Fe-TiO_2, **d** and **i** Co-TiO_2, and **e** and **j** Ni-TiO_2. **k** The plot of ratio between pre-edge peak **a** and t_{2g} peak for bare TiO_2 and the five TM-TiO_2

Figure 3a–e clearly reveals the electronic structures of the five transition metal dopants being included in anatase TiO_2 NPs. The spectrum in Fig. 3a with peaks at 576.0 and 577.0 eV with a 578.4-eV shoulder matches typical Cr^{3+} L_3-edge results for Cr-TiO_2 [27]. The sharp peak in Fig. 3b at 639.2 eV with a small feature at 640.7 eV matches other Mn^{2+} L_3-edge results [28]. The sharp peak in Fig. 3c at 708.5 eV with a small peak at 706.6 eV matches other Fe^{3+} L_3-edge results [29, 30]. The doublet in Fig. 3d at 776.8 and 777.6 eV is that of the Co^{3+} L_3-edge [27]. Finally, the sharp peak at 850.3 eV in Fig. 3e with a small peak at 852.2 eV is the typical Ni^{2+} L_3-edge spectrum [30]. These results establish the electronic states of the doped transition metals: Cr_2O_3, MnO, Fe_2O_3, Co_2O_3, and NiO, respectively.

One of our focus is to clarify the transition metal dopants induced defect structures of the TM-TiO_2 in this study. As shown in Fig. 3f–j, we can notice that the intensities for the Fe-TiO_2 and Co-TiO_2 of the two pre-edge peaks at 456.7 and 457.4 eV are higher than those of Cr-TiO_2, Mn-TiO_2, and Ni-TiO_2 (marked a) indicating that these peaks are due to surface defect structures (Ti^{3+} state) [31]. The ratios of the intensities of the pre-edge peak (a) and the t_{2g} peak are 0.11, 0.127, 0.140, 0.224, 0.238, and 0.113 for TiO_2, Cr-TiO_2, Mn-TiO_2, Fe-TiO_2, Co-TiO_2, and Ni-TiO_2, respectively (see Fig. 3k). This result means that the Ti^{3+} state is present in higher numbers in Fe-TiO_2 and Co-TiO_2.

Following the confirmation of transition metal doping by the surface analysis, we investigated band gap modulations by taking the valence-band spectra as shown in Fig. 4. The anatase TiO_2 has been reported to have a band gap of ~ 3.2 eV [32]. As shown in the valence-band spectra of Fig. 4a, the valence band maximum of TM-TiO_2 shifts lower with respect to Fermi level (E_F) from 3.10 to 1.81 eV (2.56 eV, Cr-TiO_2; 2.52 eV, Mn-TiO_2; 2.07 eV, Fe-TiO_2; 1.81 eV, Co-TiO_2; and 2.61 eV, Ni-TiO_2). From this, we can estimate that the transition metal doping gives rise to band gap narrowing because TiO_2 is highly n-type semiconductor material, and E_F in the n-type semiconductor lies close to the conduction band. Narrowing the band gap of TM-TiO_2 has resulted from its enhancement of defect structures.

As a result, we can conclude that the doped transition metals make defect structures of TiO_2 NPs and then contribute to decrease the band gap in TM-TiO_2 (in special Fe-TiO_2 and Co-TiO_2). With these understanding of variations of the structures and electronic properties for the five TM-TiO_2, we now compare the effects of transition metal doping as a point of their catalytic activities.

Electrochemical Redox Reaction in the Aqueous Phase

CVs were obtained in a PBS solution containing 0.01 M 2-ATP at various types of GCEs irradiated by 365-nm-wavelength UV light. As shown in Fig. 5g, a sluggish oxidation current is observed at a bare GCE because of the intrinsically slow oxidation of 2-ATP. To increase the current associated with the oxidation of 2-ATP, GCEs modified with the TiO_2 and TM-TiO_2-Nafion catalysts are fabricated and tested, with the results shown in Fig. 5. The currents associated with the oxidation of 2-ATP are 6.9 (± 1.4) μA and 7.1 (± 1.6) μA when using the GCEs modified with the Fe-TiO_2 and Co-TiO_2, respectively—significantly greater (i.e., 4.6 and 4.7 times greater) than the 2.0 μA value observed when using only the bare GCE (Fig. 5h). In contrast, the currents generated when using the anatase TiO_2 NPs, Cr-TiO_2, Mn-TiO_2, and Ni-TiO_2 are only 2.7 (± 0.4) μA, 4.4 (± 1.1) μA, 2.8 (± 0.5) μA, and 2.9 (± 0.7) μA, respectively, which are slightly (1.8, 2.9, 1.86, and 1.93 times) but not significantly greater than that for the bare electrode. These results reveal the importance of the type of TM-TiO_2 for catalyzing oxidation reactions, even when using small amounts (5 mol%) of the doped transition metal, and specifically indicate

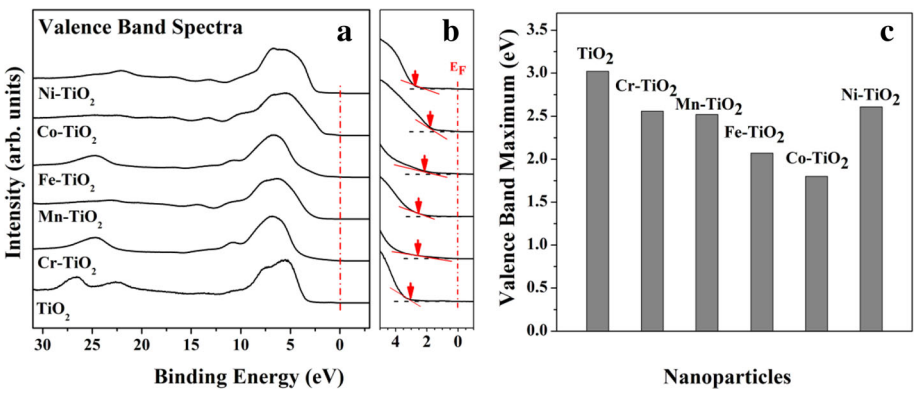

Fig. 4 **a** Valence spectra and **b** magnified view of valence band edge of anatase TiO_2 and the five TM-TiO_2. **c** The plot of valence band maximum values of TiO_2 and the five TM-TiO_2

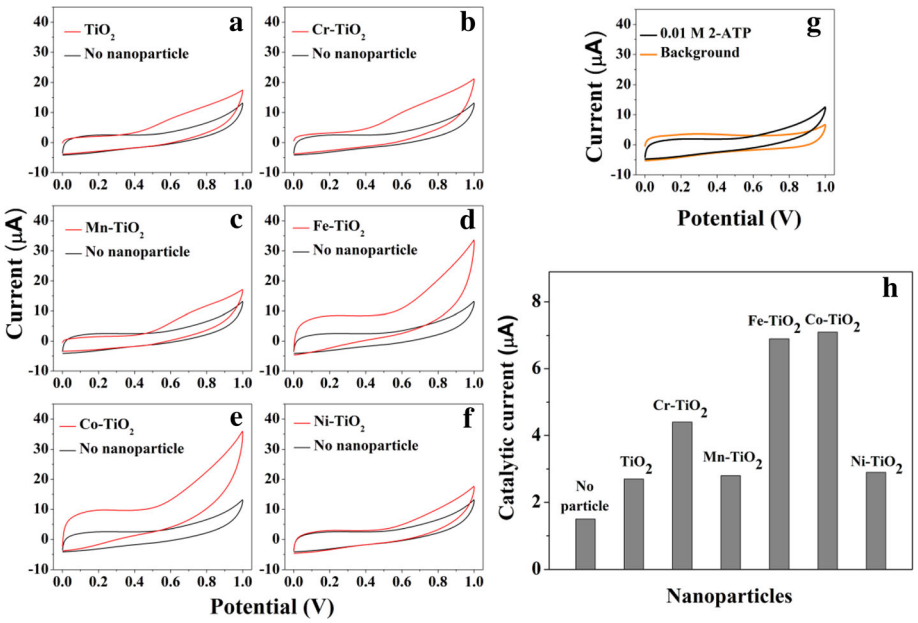

Fig. 5 a–f CVs (at a scan rate of 50 mV/s) in PBS containing 0.01 M 2-ATP at a bare GCE (black lines) or GCEs modified (red lines) with 5 mol% **a** anatase TiO_2, **b** Cr-TiO_2, **c** Mn-TiO_2, **d** Fe-TiO_2, **e** Co-TiO_2, and **f** Ni-TiO_2. **g** A sluggish oxidation current observed at a bare GCE because of the intrinsically slow oxidation of 2-ATP. **h** Catalytic currents resulting from the electrochemical oxidation of 2-ATP for the various types of anatase TiO_2 and the five TM-TiO_2

the Fe-TiO_2 and Co-TiO_2 to be good catalysts for the oxidation of 2-ATP.

Photocatalytic Oxidation of 2-ATP

We also determined the direct catalytic activities of the TM-TiO_2 in the oxidation of 2-ATP molecules. The S 2*p* core-level spectra of anatase TiO_2 and 5 mol% TM-TiO_2 were obtained with HRPES after 180 l of 2-ATP exposure in the presence of oxygen under 365 nm UV light illumination (see Fig. 6a–f). These spectra contain three distinct $2p_{3/2}$ peaks at 161.5, 162.9, and 168.6 eV, which are assigned to S1, the C-SH unbounded state, S2, the bound state, and S3, sulfonic acid (SO_3H), respectively. It is well known that sulfonic acid is an oxidation product of thiol groups [33, 34]. Hence, we can monitor the oxidation of 2-ATP by measuring the ratio of the intensities of peaks S3 and S1. Figure 6a–f confirms that Fe-TiO_2 and Co-TiO_2 act as effective photocatalysts. The ratios of the intensities are 0.07, 0.12, 0.10, 0.27, 0.29, and 0.08 for anatase TiO_2 NPs, Cr-TiO_2, Mn-TiO_2, Fe-TiO_2, Co-TiO_2, and Ni-TiO_2, respectively, i.e., the ratios of Fe-TiO_2 and Co-TiO_2 are also higher than those of the other nanoparticles (see Fig. 6g). This result is closely correlated with the number of defect structures in the TM-TiO_2 shown in Fig. 3. In the STXM measurements, we confirm that Fe-TiO_2 and Co-TiO_2 contain more Ti^{3+} defect states (i.e., surface defect structures). Thus, these results indicate that increasing the number of Ti^{3+} defect structures is closely correlated with the enhancement of catalytic activity [7]. As a result, the Fe-TiO_2 and Co-TiO_2, which contain many Ti^{3+} defect states, have higher catalytic activities.

For this reason, we can consider three factors (charge state dependence, surface defect structure dependence, and hybridization between the doped transition metals and TiO_2), which can cause the enhancement of catalytic activities of TM-TiO_2. At first, the effect of electronic charge state has been also investigated by using STXM measurement. As shown in Fig. 3a–e, we confirm that Cr, Fe, and Co transition metal ions have the TM^{3+} charge states, while Mn and Ni have the TM^{2+} charge states. Therefore, we can conclude that there is no correlation between electron charge states of dopants and catalytic activity of TM-TiO_2. Secondly, we checked the surface defect structure dependence. Comparing the ratio of the intensities of the pre-edge peak (A) and the t_{2g} peak shown in Fig. 3, we confirm that the number of surface defect structure is in order of Co-TiO_2 > Fe-TiO_2 > Mn-TiO_2 > Cr-TiO_2 > Ni-TiO_2 > TiO_2. As previously stated, Fe-TiO_2 and Co-TiO_2 exhibit clear enhancement in catalytic activity. With increasing surface defect structures, the catalytic activities of TM-TiO_2 increase. By monitoring the pre-edge ratios, we observed clear surface defect structure dependence in enhancing catalytic activity. Consequentially, the surface defect structure only influences on enhancement of catalytic activity of TM-TiO_2.

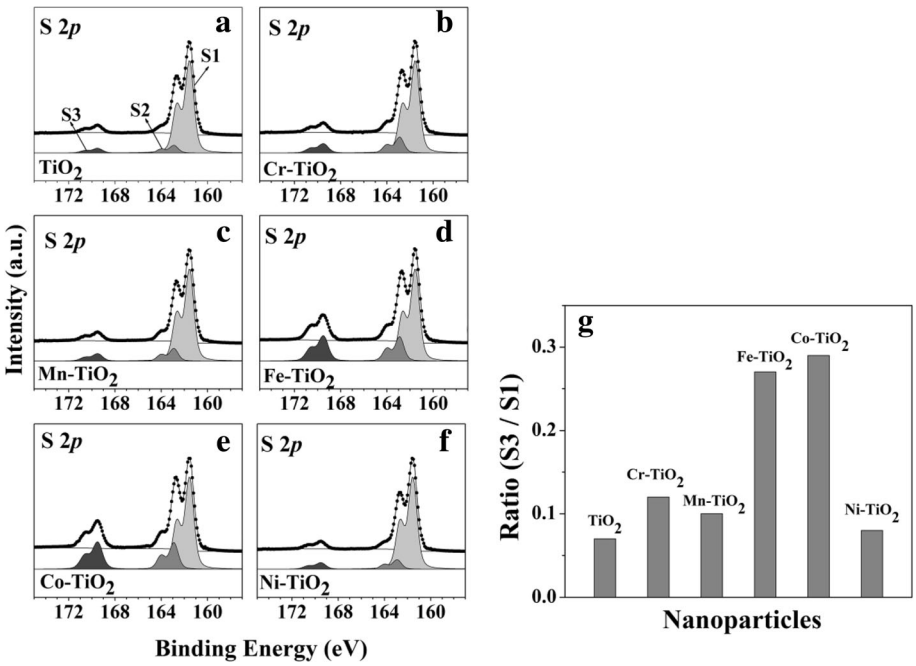

Fig. 6 (Left panel) HRPES S 2*p* core-level spectra obtained after the catalytic oxidations of 180 L 2-ATP (the saturation exposure in our system) on anatase TiO_2 and 5 mol% TM-TiO_2 (**a** TiO_2, **b** Cr-TiO_2, **c** Mn-TiO_2, **d** Fe-TiO_2, **e** Co-TiO_2, and **f** Ni-TiO_2). (Right panel) **g** The plot for intensity ratio between S3 (− SO_3H) and S1 (− SH) of anatase TiO_2 and the five TM-TiO_2, indicating their catalytic activities in the oxidation of 2-ATP, for 180-l exposures under 365 nm UV light

Finally, another reasonable explanation is that according to the O *K*-edge XAS shown in Fig. 2, a higher proportion of less-hybridized oxygen states (538 and 543 eV) appears in Fe-TiO_2 and Co-TiO_2 than in the other TM-TiO_2. Those transition of the doped transition metal 3*d* to the O 2*p* unoccupied state can facilitate the removal of oxygen atoms from the TiO_2 nanoparticles and enhance the catalytic oxidation of 2-ATP because oxygen vacancy site of TiO_2 is an active site. Conclusively, doping the TiO_2 nanoparticle with either Fe or Co yields a higher increase in the catalytic activities for 2-ATP oxidation than doping with Cr, Mn, or Ni.

Conclusions

TM-TiO_2 synthesized with a thermo-synthesis method were examined with various surface analysis techniques. To compare the catalytic activities of the five TM-TiO_2 with the anatase TiO_2 NPs, we monitored their effects on the photocatalytic oxidation of 2-ATP molecules by using HRPES and oxidation of 2-ATP by using EC measurements. Depending on the doped transition metals, we clearly investigated that the increased defect structures and less hybridization induced by the doped transition metals affect the enhanced catalytic activities. In particular, Fe^{3+} and Co^{3+} ions generate more effective oxidation state discrepancies, i.e., more Ti^{3+} defect structures and surface transformations than the other metal ions (Cr^{3+}, Mn^{2+}, and Ni^{2+}). As a result, we figured out that the catalytic properties of Fe-TiO_2 and Co-TiO_2 are superior to those of anatase TiO_2 NPs and other TM-TiO_2 (TM=Cr, Mn, and Ni).

Abbreviations

HRPES: High-resolution photoemission spectroscopy; SEM: Scanning electron microscopy

Acknowledgements

This research was supported by the National Research Foundation of Korea (NRF) funded by the Korean government (MSIP) (No. 2017R1A2A2A05001140). Additionally, this research is financially supported by the Ministry of Trade, Industry and Energy (MOTIE), and Korea Institute for Advancement of Technology (KIAT) through the International Cooperative R&D program (N053100009, "Horizon2020 Kor-EU collaborative R&BD on ACEnano Toolbox") as part of the European Commission Horizon 2020 Programme under grant agreement NMBP-26-2016-720952.

Authors' Contributions

SY and HL, who is the corresponding author, participated in overall experiments. Both authors read and approved the final manuscript.

Competing Interests

The authors declare that they have no competing interests.

Publisher's Note

Author details
[1]Center for Nano Characterization, Korea Research Institute of Standards and Science, Daejeon 305-400, Republic of Korea. [2]Department of Chemistry, Sookmyung Women's University, Seoul 140-742, Republic of Korea.

Received: 20 July 2017 Accepted: 25 October 2017
Published online: 03 November 2017

References

1. Qiu Y, Chen W, Yang S (2010) Double-layered photoanodes from variable-size anatase TiO_2 nanospindles: a candidate for high-efficiency dye-sensitized solar cells. Angew Chem Int Ed 122:3757–3761
2. Pang CL, Lindsay R, Thornton G (2008) Chemical reactions on rutile TiO_2(110). Chem Soc Rev 37:2328–2353
3. Liu B, Aydil ES (2009) Growth of oriented single-crystalline rutile TiO_2 nanorods on transparent conducting substrates for dye-sensitized solar cells. J Am Chem Soc 131:3985–3990
4. Woolerton TW, Sheard S, Reisner E, Pierce E, Ragsdale SW, Armstrong FA (2010) Efficient and clean photoreduction of CO_2 to CO by enzyme-modified TiO_2 nanoparticles using visible light. J Am Chem Soc 132:2132–2133
5. Ma Y, Wang X, Jia Y, Chen X, Han H, Li C (2014) Titanium dioxide-based nanomaterials for photocatalytic fuel generations. Chem Rev 114:9987–10043
6. Waterhouse GIN, Wahab AK, Al-Oufi M, Jovic V, Anjum DH, Sun-Waterhouse D, Llorca J, Idriss H (2013) Hydrogen production by tuning the photonic band gap with the electronic band gap of TiO_2. Sci Rep 3:2849
7. Hwang YJ, Yang S, Jeon EH, Lee H (2016) Photocatalytic oxidation activities of TiO_2 nanorod arrays: a surface spectroscopic analysis. Appl. Cat. B: Environ. 180:480–486
8. Kaden WE, Wu T, Kunkel WA, Anderson SL (2009) Electronic structure controls reactivity of size-selected Pd clusters adsorbed on TiO_2 surfaces. Science 326:826–829
9. Inturia SNR, Boningaria T, Suidanb M, Smirniotisa PG (2014) Visible-light-induced photodegradation of gas phase acetonitrile using aerosol-made transition metal (V, Cr, Fe, Co, Mn, Mo, Ni, Cu, Y, Ce, and Zr) doped TiO_2. Appl. Cat. B: Environ. 144:333–342
10. Yang S, Jeon EH, Kim Y, Baik J, Kim N, Kim H, Lee H (2016) Toward enhancement of TiO_2 surface defect sites related to photocatalytic activity via facile nitrogen doping strategy. Cat Comm 81:45–49
11. Tryba B, Morawski AW, Inagaki M, Toyoda M (2006) The kinetics of phenol decomposition under UV irradiation with and without H_2O_2 on TiO_2, Fe-TiO_2 and Fe-C-TiO_2 photocatalysts. Appl Cat B: Environ 63:215–221
12. Eschemann TO, Jong KP (2015) Deactivation behavior of Co/TiO_2 catalysts during Fischer–Tropsch synthesis. ACS Catal 5:3181–3188
13. Xu Y, Zhou M, Wen L, Wang C, Zhao H, Mi Y, Liang L, Fu Q, Wu M, Lei Y (2015) Highly ordered three-timensional Ni-TiO_2 nanoarrays as sodium ion battery anodes. Chem Mater 27:4274–4280
14. Chen WT, Chan A, Sun-Waterhouse D, Moriga T, Idriss H, Waterhouse GIN (2015) Ni/TiO_2: a promising low-cost photocatalytic system for solar H_2 production from ethanol–water mixtures. J Catal 326:43–53
15. Manu S, Khadar MA (2015) Non-uniform distribution of dopant iron ions in TiO_2 nanocrystals probed by X-ray diffraction, Raman scattering, photoluminescence and photocatalysis. J Mater Chem C 3:1846–1853
16. Yan J, Zhang Y, Liu S, Wu G, Li L, Guan N (2015) Facile synthesis of an iron doped rutile TiO_2 photocatalyst for enhanced visible-light-driven water oxidation. J Mater Chem A 3:21434–21438
17. Li X, Guo Z, He T (2013) The doping mechanism of Cr into TiO_2 and its influence on the photocatalytic performance. Phys Chem Chem Phys 15: 20037–20045
18. Ould-Chikh S, Proux O, Afanasiev P, Khrouz L, Hedhili MN, Anjum DH, Harb M, Geantet C, Basset JM, Puzenat E (2014) Photocatalysis with chromium-doped TiO_2: bulk and surface doping. ChemSusChem 7:1361–1371
19. Rashad MM, Elsayed EM, Al-Kotb MS, Shalan AE (2013) The structural, optical, magnetic and photocatalytic properties of transition metal ions doped TiO_2 nanoparticles. J Alloys Compd 581:71–78
20. Siddhapara KS, Shah DV (2014) Experimental study of transition metal ion doping on TiO_2 with photocatalytic behavior. J Nanosci Nanotechnol 14: 6337–6341
21. Wang D, Liu L, Sun X, Sham TK (2015) Observation of lithiation-induced structural variations in TiO_2 nanotube arrays by X-ray absorption fine structure. J Mater Chem A 3:412–419
22. Hwu Y, Yao YD, Cheng NF, Tung CY, Lin HM (1997) X-ray absorption of nanocrystal TiO_2. Nanostruct Mater 9:355–358
23. Krüger P (2010) Multichannel multiple scattering calculation of $L_{2,3}$-edge spectra of TiO_2 and $SrTiO_3$: importance of multiplet coupling and band structure. Phys Rev B 81:125121
24. Thomas AG, Flavell WR, Mallick AK, Kumarasinghe AR, Tsoutsou D, Khan N, Chatwin C, Rayner S, Smith GC, Stockbauer RL, Warren S, Johal TK, Patel S, Holland D, Taleb A, Wiame F (2007) Comparison of the electronic structure of anatase and rutile TiO_2 single-crystal surfaces using resonant photoemission and x-ray absorption spectroscopy. Phys Rev B 75:035105
25. Yan W, Sun Z, Pan Z, Liu Q, Yao T, Wu Z, Song C, Zeng F, Xie Y, Hu T, Wei S (2009) Oxygen vacancy effect on room-temperature ferromagnetism of rutile Co:TiO_2 thin films. Appl Phys Lett 94:042508
26. Tian F, Zhang Y, Zhang J, Pan C (2012) Raman spectroscopy: a new approach to measure the percentage of anatase TiO_2 exposed (001) facets. J Phys Chem C 116:7515–7519
27. Meyers D, Mukherjee S, Cheng JG, Middey S, Zhou JS, Goodenough JB, Gray BA, Freeland JW, Saha-Dasgupta T, Chakhalian J (2013) Zhang-Rice physics and anomalous copper states in A-site ordered perovskites. Sci Rep 3:1834
28. Qiao R, Chin T, Harris SJ, Yan S, Yang W (2013) Spectroscopic fingerprints of valence and spin states in manganese oxides and fluorides. Curr Appl Phys 13:544–548
29. Liu X, Wang D, Liu G, Srinivasan V, Liu Z, Hussain Z, Yang W (2013) Distinct charge dynamics in battery electrodes revealed by in situ and operando soft X-ray spectroscopy. Nat Commun 4:2568
30. Kleiner K, Melke J, Merz M, Jakes P, Nagel P, Schuppler S, Liebau V, Ehrenberg H (2015) Unraveling the degradation process of LiNi0.8Co0.15Al0. 05O2 electrodes in commercial lithium ion batteries by electronic structure investigations. ACS Appl. Mater. Interfaces 7:19589–19600
31. Kareev M, Prosandeev S, Liu J, Gan C, Kareev A, Freeland JW, Xiao M, Chakhalian J (2008) Atomic control and characterization of surface defect states of TiO_2 terminated $SrTiO_3$ single crystals. Appl Phys Lett 93:061909
32. Dette C, Perez-Osorio MA, Kley CS, Punke P, Patrick CE, Jacobson P, Giustino F, Jung SJ, Kern K (2014) TiO_2 anatase with a bandgap in the visible region. Nano Lett 14:6533–6538
33. Rodella CB, Barrett DH, Moya SF, Figueroa SJA, Pimenta MTB, Curvelo AAS, Teixeira da Silva V (2015) Physical and chemical studies of tungsten carbide catalysts: effects of Ni promotion and sulphonated carbon. RSC Adv 5: 23874–23885
34. Suganuma S, Nakajima K, Kitano M, Yamaguchi D, Kato H, Hayashi S, Hara M (2008) Hydrolysis of cellulose by amorphous carbon bearing SO_3H, COOH, and OH groups. J Am Chem Soc 130:12787–12793